Clays and Clay Minerals, Vol. 41, No. 2, 191–208, 1993.

EXPERIMENTAL DETERMINATION OF THE RATES OF PRECIPITATION OF AUTHIGENIC ILLITE AND KAOLINITE IN THE PRESENCE OF AQUEOUS OXALATE AND COMPARISON TO THE K/Ar AGES OF AUTHIGENIC ILLITE IN RESERVOIR SANDSTONES

J. S. SMALL

Department of Geology, University of Manchester, Manchester M13 9PL, U.K.

Abstract—The importance of precipitation rate as an effective control on illite and kaolanite formation during diagenesis has been examined by measuring precipitation rates, from Al fluid concentration, in a Dickson fluid-sampling vessel at 160°–250° and 500 bars (50 MPa). These experiments are considered to be analogues of the precipitation of clays in sandstones from porewaters containing dissolved carboxylic acids, which have a transient stability and may influence aluminosilicate solubility. Precipitated illite had a lath-shaped morphology and its composition was consistent with authigenic illite in sandstones. Kaolinite formed tabular rather than vermicular shaped crystals. Kaolinite precipitation rate was two orders of magnitude faster than illite precipitation and was rate-limited by the decomposition of oxalate; kaolinite formation should be equilibrium-controlled at virtually all stages of burial. Extrapolation of illite precipitation rate to burial temperatures indicates that the first appearance of illite in a burial sequence may be kinetically controlled. A model of illite precipitation based on these experimental results has been used to predict the time required to precipitate illite during burial of a sandstone, taking into account temperature changes during burial. For northern North Sea examples, a predicted illitization threshold of −60°C occurring at 60–80 Ma corresponds to the observed initiation of authigenic illite precipitation. Times of around 2–5 Ma would be required to reach a 98% approach to equilibrium at this threshold. The main phase of illite precipitation in the northern North Sea basin is a later, hydrologically controlled event (30–50 Ma). Equilibrium would be approached in around 0.1 Ma during this phase, which is consistent with the narrow illite K/Ar age range (1–5 Ma) recorded for some sequences.

Key Words—Illite, Kaolinite, Precipitation rate, Oxalate, K/Ar, Sandstones, North Sea.

INTRODUCTION

Clay mineral formation reactions during burial diagenesis are controlled thermodynamically by changed mineral stability in response to variation in temperature and fluid composition, and kinetically by the rate at which clay reactions occur relative to the time scales of burial and fluid movement. In order to predict the time and temperature at which clay mineral reactions occur, it is vital that both the thermodynamics and kinetics of these reactions are understood. Reaction rates are directly dependent on temperature, and at temperatures <100°C silicate reactions may be effectively kinetically controlled. The aim of this study is to estimate the rate of illite and kaolinite precipitation from solution at diagenetic temperatures in order to evaluate the possible kinetic constraints on the depth/temperature of formation.

The kinetics of the smectite to illite reaction during shale diagenesis (Hower *et al.*, 1976) have been studied extensively using experimental techniques (Eberl and Hower, 1976; Roberson and Lahann, 1981; Inoue, 1983; Howard and Roy, 1983; Whitney and Northrop, 1988; Whitney, 1990). Huang *et al.* (1991) have shown that illite/smectite composition versus depth profiles can be calculated using an experimentally derived kinetic model assuming knowledge of pore fluid K concentration.

Recently, experimental studies relevant to authigenic clay formation in sandstones have been carried out using a variety of methods studying both the stability and kinetics of clay mineral formation. Huang *et al.* (1986) synthesised illite and kaolinite following HCl dissolution of feldspar at 200°C and derived a model for illite and kaolinite authigenesis based on closed system titration of acidic fluids by feldspar. Sass *et al.* (1987) and Aja *et al.* (1991) re-examined illite and illite/smectite stability by a solubility study of natural illite-bearing assemblages between 60°C and 250°C. Chermak and Rimstidt (1990) performed a kinetic investigation of the alteration of kaolinite to illite in KCl solution between 250°C and 307°C and monitored the reaction by variation in quench pH. Nagy *et al.* (1991) measured kaolinite dissolution and precipitation rate at 80°C using a flow cell apparatus, where precipitation of kaolinite was inferred from comparison of input and output fluid composition. Small *et al.* (1992a, 1992b) showed with a series of batch experiments that illite and kaolinite could be precipitated between 150°C and 350°C on a sandstone substrate following dissolution of aluminosilicate gels and mineral phases. Illite and kaolinite produced in this way are representative of the

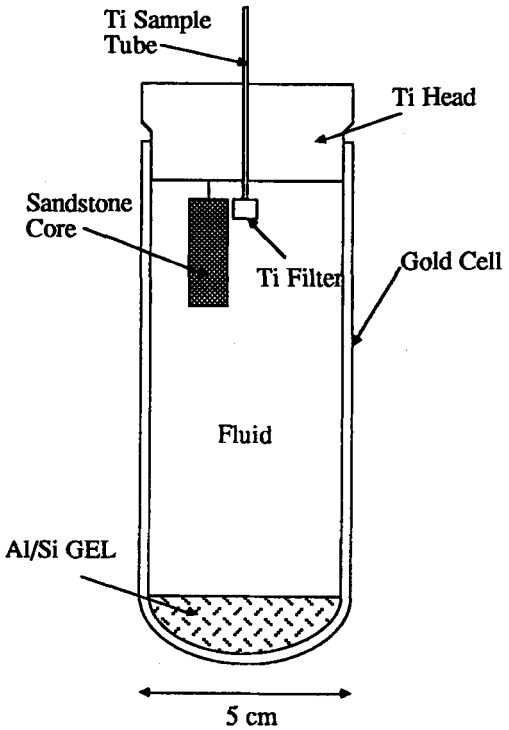

Figure 1. Gold/titanium cell used in fluid sampling experiments.

morphology and composition of authigenic clays formed in sandstones. Small and Manning (1993) repeated illite precipitation experiments in a Dickson fluid-sampling apparatus where dissolution and precipitation were monitored from the composition of fluids withdrawn at intervals during the experiment. These fluid composition data could then be interpreted with the mineralogical analyses of the solid products to examine controls on illite morphology and to define authigenic illite stability.

The potential effect of aqueous carboxylic acid anions in controlling aluminosilicate solubility has received considerable attention in the last decade. Dicarboxylic anions such as oxalate have been proposed as important complexing agents for aluminium in soils (Huang and Keller, 1970; Antweiler and Drever, 1983), and during diagenesis, where aqueous organic species are released during hydrocarbon maturation in mudrocks (Surdam *et al.*, 1984, 1989), and from petroleum accumulations in reservoirs (MacGowan and Surdam, 1990; Boles, 1992). The dicarboxylic acid anion malonate is recorded in oil field waters at concentrations up to 2500 mg/l while oxalate has a maximum recorded concentration of 100 mg/l (MacGowan and Surdam, 1988). Monocarboxylic acid anions such as acetate and propanoate are recorded at higher concentrations than the dicarboxylic anions. Crossey (1991) has measured the rate of decomposition of oxalate and shown that oxalate is considerably more unstable than acetate and that pH is a major control on decomposition rate. Small (1993) has shown that lower redox potential decreases oxalate decomposition rate and that mineral catalysis may increase decomposition rate. Given the unstable nature of dicarboxylic acid anions during diagenesis and the limited number of analyses of carboxylic acid anions, it is possible that the recorded maximum concentrations do not represent the concentration of these species when they actively control diagenetic dissolution and precipitation reactions.

Our previous experiments (Small *et al.*, 1992b; Small and Manning, 1993) showed that oxalate enhanced clay precipitation and in the case of illite promoted the formation of fibrous rather than platy illite. The effect of oxalate in these clay precipitation experiments is to increase Al solubility and also to increase the rate of dissolution of the Al/Si gel (Small and Manning, 1993). Speciation modeling shows that oxalate forms a dimeric Al-oxalate complex under acidic conditions. At oxalate concentrations between 10 and 900 mg/l (Small, 1992, 1993), this complex increases the solubility of kaolinite by 2–3 orders of magnitude. Under alkaline conditions, where illite is precipitated, Al-oxalate is not significant, and measured solubilities can be accounted for by the species $Al(OH)_4^-$. The observation is made in these experiments that enhanced clay precipitation associates the initial dissolution in the presence of oxalate and the subsequent degradation of oxalate; under acidic conditions, kaolinite precipitation results from the breakdown of an Al-oxalate complex, while under alkaline conditions illite precipitation results from the decrease in pH that associates the breakdown of oxalate to CO_2 and formate.

This paper presents mineralogical and fluid composition data of fluid-sampling experiments carried out at a series of temperatures between 160°C and 250°C where the rate of precipitation of illite and kaolinite from an oxalate-bearing fluid is determined from changing Al concentration. These experiments are considered to be analogues of mineral dissolution and clay precipitation in organic-rich pore waters where carboxylic acid anions have a transient stability. The initial oxalate concentration used (880 mg/l) is considerably higher than that measured in natural pore waters; however, the final concentration after oxalate breakdown and associated clay precipitation is well within the range of recorded analyses. Estimation of the rate of precipitation at diagenetic temperatures is made by extrapolation using an Arrhenius equation. The precipitation rate of natural authigenic illite in sandstone that is predicted from these experiments is compared to K/Ar ages of illites in some North Sea sandstone reservoirs to validate the experimental results and to estimate the likely age range represented by K/Ar illite ages.

EXPERIMENTAL METHODS

Fluid sampling experiments were carried out in a Dickson fluid-sampling autoclave supplied by Core-Test Systems Inc., Mountain View, California. A 200 ml gold reaction cell with titanium closure, sampling tube, and sampling valve were used identical to that described by Seyfried *et al.* (1987). Experiments were performed at 500 bars (50 MPa) between 160°C and 250°C. The furnace and pressure vessel were rocked continuously through an angle of 120°, thus ensuring mixing of fluid and equilibration of temperature. Run temperatures and starting materials (Table 1) were selected in consideration of previous experiments (Small *et al.,* 1992a, 1992b; Small and Manning, 1993) and were designed to precipitate either illite or kaolinite. Both illite and kaolinite precipitation experiments initially dissolve an Al/Si gel. 1 g of Al/Si gel was reacted with 200 ml of aqueous solution. The illite experiments contained a core of sandstone that was originally free of authigenic clay to act as a substrate for nucleation. Cores measured 8 mm diameter, 40 mm length and were suspended in the fluid phase (Figure 1). The sandstone substrate was not included in the kaolinite experiments because preliminary experiments had shown that, in the initially acidic conditions used (pH 2), high concentrations of Fe were produced (20 mg/l) following dissolution of hematite, which might result in the precipitation of phases other than kaolinite.

Materials

An aluminosilicate gel starting material of composition $Al_2O_3 \cdot 2SiO_2$ was prepared by the method of Hamilton and Henderson (1968). The surface area of the sintered gel determined by the BET method, using nitrogen, was 0.4 m^2/g. X-ray diffraction (XRD) showed that the sintered gel was partially crystallised to mullite, producing broad peaks of spacing 5.40 Å and 3.42 Å. Starting solutions used (Table 1) were made up from analytical grade reagents. The sandstone substrate used in the illite experiments was a sample of Penrith Sandstone, a high-porosity, high-permeability authigenic clay-free quartz-arenite from Stoneraise Quarry, Cumbria, England. This sandstone was chosen for its absence of authigenic clays so that synthetic clays could be unambiguously identified. The major cementing phase is quartz, occurring as well developed overgrowths. Petrographic and XRD study has shown that small quantities of feldspar (5%) and lithic fragments (2%) are present in the sample, which contribute some detrital clay. Infiltrated/detrital clay and Fe hydroxide/hematite coatings are present on the grain surfaces of abraded grains. Small *et al.* (1992a) discusses how these coatings can influence the nucleation of synthetic clays.

Analysis of solid products

The morphology of clays precipitated on the surface of the sandstone core and in the post-run gel was examined in detail by secondary electron scanning electron microscopy (SEM) and their composition was characterised qualitatively from energy dispersive X-ray spectra. XRD was used to examine the post-run gel using CuKα radiation at a scan rate of 1°2θ/min. XRD samples were prepared by air drying on a glass slide a suspension produced by light grinding and ultrasonic disaggregation of the gel for 2 min. Analytical transmission electron microscopy (ATEM) was used to obtain accurate single grain analyses of illite particles and to examine clay morphology. TEM samples were prepared from a fine fraction of dispersed clay from the outside of the sandstone core. An approximate <2 μm clay fraction was prepared by ultrasonic disaggregation of a portion of the core in 5 ml of deionised water followed by settling for 5 min. A diluted drop of the fine clay fraction was dried on a carbon film mounted on a Cu TEM grid, and ATEM analyses were made using a Phillips 400T TEM/STEM with EDAX energy dispersive X-ray analysis. X-ray spectra were collected from electron transparent clay particles at 100 kV for 100 seconds and processed by the method of Cliff and Lorimer (1975). Calibration factors were determined from independently analysed macroscopic micas.

Table 1. Starting solutions and run conditions of experiments.

Experiment	Temp., °C	Duration (hr)	Starting solution
Kaolinite experiments			
R11	200	936	0.01 M oxalic acid, 0.01 M KCl
R13	160	840	0.01 M oxalic acid, 0.01 M KCl
R14	180	123	0.01 M oxalic acid, 0.01 M KCl
Illite experiments			
R2	250	241	0.01 M K-oxalate
R3	250	48	0.01 M K-oxalate
R5	200	960	0.01 M K-oxalate
R6	200	725	0.01 M K-oxalate
R9	230	1706	0.01 M K-oxalate

Fluid analyses

Eight ml samples of fluid were recovered at irregular intervals (Table 2), measured from the start of furnace heating, and passed through a 0.2 μm syringe filter. A 1 ml aliquot was immediately diluted 10 times in deionised water to avoid precipitation of silica and alumina on standing prior to analysis, although in practice no precipitate was observed. The pH was determined immediately on the undiluted aliquot under a nitrogen atmosphere with a Microelectrodes Inc. 1 drop electrode calibrated to pH 4 and 7. The major soluble elements of interest in this study are Si, Al, and K. Si, Al, and K concentrations were determined on both aliquots by ICP atomic emission spectroscopy (ICP); in addition, some K analyses were checked by flame atomic absorption spectroscopy (AAS). Al concentration was determined in the undiluted aliquot by ICP

https://doi.org/10.1346/CCMN.1993.0410208 Published online by Cambridge University Press

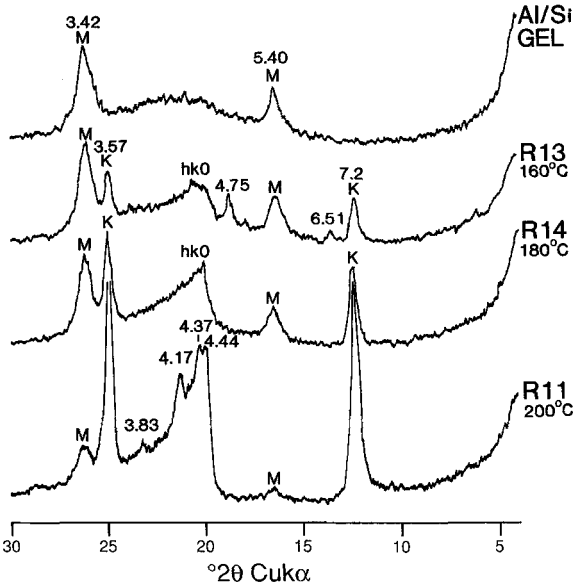

Figure 2. X-ray diffraction patterns (CuKα radiation) of starting gels and kaolinite formed in experiments R11, R13, and R14. Specimens are whole samples of post-run gel. K = kaolinite, M = mullite, d spacing in Å.

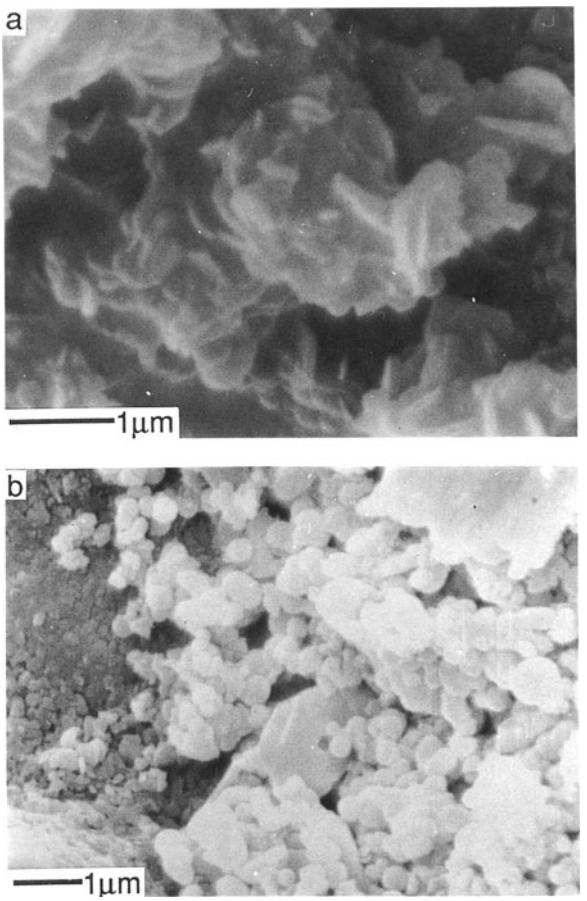

Figure 3. Scanning electron micrographs of kaolinite precipitated on the Al/Si starting gel following dissolution in 0.01 M oxalic acid and 0.01 M KCl: a) experiment R11, 200°C; b) experiment R13, 160°C.

down to a detection limit of 0.2 mg/l, Si and K were well above detection limits in all samples. Trace elements concentrations (Fe, Mg, Ca, and Na) were analysed on the undiluted aliquot by ICP. Anion concentrations were analysed by ion chromatography using a Dionex AS5A anion separator column. Anions of interest were oxalate, acetate, and formate. All analyses were performed within 3 days of sampling; samples were stored at 5°C to avoid bacterial breakdown of the organics. Freezing of the sample was avoided, since this resulted in precipitation of silica. Fluid analyses are presented in Table 2.

RESULTS AND DISCUSSION

Kaolinite precipitation

Kaolinite was formed in experiments with a starting solution of 0.01 M oxalic acid plus 0.01 M KCl (R11, R13, and R14). XRD patterns of post-run gels from experiments R11, R13, and R14 and the starting gel are shown in Figure 2. With increasing temperature of reaction, there was an increase in the intensity of the kaolinite basal 7 Å and 3.5 Å peaks. In all samples, hk0 maxima were resolved at 19.9°2θ. This results from poor orientation of the sample and is a common feature of synthetic clays formed from gels (Small *et al.*, 1992a). The hk0 peaks increase in intensity with reaction temperature and, in the 200°C experiment (R11), peaks are resolved of 4.44 Å, 4.37 Å, 4.17 Å, and 3.83 Å. The hk0 peaks at 3.83 Å, 2.34 Å, and 2.30 Å in R11 identify the kaolinite polymorph (Bailey, 1980). The poor resolution of the hk0 peaks in the two lower temperature experiments is interpreted as a result of increased layer stacking disorder (Brindley, 1980). It is likely that increased ordering will account for a proportion of the increased basal intensity with temperature. However, mullite peaks at 5.40 Å and 3.42 Å decrease in intensity as kaolinite intensity increases, indicating greater alteration of mullite to kaolinite with higher temperature. Two small peaks are present in R13 at 6.51 Å and 4.75 Å. These may represent metastable Al-oxyhydroxide phases pseudoboehmite and nordstrandite. ATEM examination of the post-run gel showed that some euhedral grains were present, which were mainly composed of Al with <10 mole% S. These grains were unstable under the electron beam and possibly represent Al-oxyhydroxides formed during Al precipitation.

SEM examination of the post-run gel of the 200°C experiment (R11) (Figure 3a) revealed that ~0.5 μm diameter hexagonal kaolinite plates have formed. The plates appeared to be coated and in some cases are poorly resolved from the ground mass of the gel. This coating could not be removed by washing in deionised

https://doi.org/10.1346/CCMN.1993.0410208 Published online by Cambridge University Press

Table 2. Analyses of fluid samples recovered from illite and kaolinite precipitation experiments.

Sample	Time (h)	T°C	Si mg/l	Al mg/l	K mg/l	Na mg/l	Ca mg/l	Mg mg/l	Fe mg/l	pH 25°C	Oxalate mg/l	Formate mg/l
R2s	0	25	2.6	8.96	644	n.d.	0.80	n.d.	0.08	7.45	800	n.d.
R2a	2	100	4.3	12.41	651	n.d.	0.09	0.12	0.08	7.61	755	n.d.
R2b	4	175	30.4	25.98	624	n.d.	n.d.	0.14	0.04	7.40	849	n.d.
R2c	7	250	113.5	30.42	534	n.d.	n.d.	0.04	n.d.	6.92	172	265
R2d	24	256	200.7	2.85	269	0.34	0.02	0.01	n.d.	6.08	11	192
R2e	49	249	168.1	1.23	183	n.d.	0.04	0.01	n.d.	6.07	n.d.	87
R2f	72	250	164.2	1.52	156	n.d.	n.d.	n.d.	n.d.	6.01	n.d.	46
R2g	97	250	166.3	1.80	132	n.d.	n.d.	n.d.	n.d.	6.24	n.d.	31
R2h	168	249	182.9	1.77	104	n.d.	n.d.	n.d.	n.d.	6.22	n.d.	28
R2i	241	249	196.3	1.62	85	n.d.	n.d.	n.d.	n.d.	6.36	n.a.	n.a.
R3s	0	25	0.1	n.d.	742	n.d.	0.15	0.01	0.16	6.94	800	n.d.
R3a	1	40	1.5	2.84	725	n.d.	0.13	0.08	0.15	7.19	810	n.d.
R3b	4	100	4.3	7.59	692	n.d.	0.16	0.09	0.11	7.89	811	n.d.
R3c	5	180	25.8	20.04	646	0.01	0.20	0.11	0.13	7.55	803	n.d.
R3d	8	249	110.4	29.80	550	0.26	n.d.	0.07	0.12	7.26	313	228
R3e	12	266	177.3	34.90	462	0.13	n.d.	n.d.	n.d.	7.11	6	397
R3f	16	251	192.4	19.80	403	0.10	n.d.	n.d.	n.d.	6.83	n.d.	363
R3g	20	248	204.0	10.22	407	n.d.	n.d.	n.d.	n.d.	6.99	n.d.	352
R3h	24	249	202.0	6.91	368	n.d.	n.d.	n.d.	n.d.	6.68	n.d.	343
R3i	29	249	206.9	4.42	333	n.d.	n.d.	n.d.	n.d.	6.65	n.d.	322
R3j	48	256	195.5	2.24	250	n.d.	n.d.	n.d.	n.d.	6.56	n.d.	235
R5a	0	25	1.6	1.14	730	1.41	0.15	0.10	0.07	6.82	853	n.d.
R5b	2	100	1.9	1.72	770	0.47	0.18	0.17	0.07	6.67	885	n.d.
R5c	7	200	22.1	6.53	810	1.07	0.16	0.17	0.03	8.55	767	n.d.
R5d	13	197	92.4	15.81	780	1.33	0.23	0.20	0.10	8.11	664	32
R5e	24	196	112.6	17.57	750	1.29	0.24	0.15	0.05	8.10	484	129
R5f	48	200	114.8	17.29	720	1.62	0.18	0.07	0.02	7.73	295	243
R5g	72	200	118.7	17.33	710	1.85	0.11	0.03	0.01	8.03	179	303
R5h	144	200	123.2	16.38	705	1.41	0.01	n.d.	n.d.	6.58	54	346
R5i	240	200	126.8	14.84	700	1.12	n.d.	n.d.	n.d.	7.00	7	352
R5j	960	201	110.0	0.10	278	2.35	0.06	n.d.	n.d.	6.76	3	263
R5fin	970	25	103.0	n.d.	272	0.90	0.60	n.d.	n.d.	6.72	n.a.	n.a.
R6a	30	200	101.9	21.43	757	1.89	0.29	0.10	0.05		492	129
R6b	150	198	109.5	17.63	735	1.27	0.02	0.01	n.d.	7.58	91	317
R6c	319	199	117.4	16.19	693	1.49	0.09	0.02	n.d.	7.61	9	329
R6d	509	199	119.8	13.82	686	1.43	0.07	0.02	n.d.	7.58	4	285
R6e	725	200	135.8	11.32	656	1.16	n.d.	n.d.	n.d.	7.55	4	270
R6fin	735	25	97.6	0.85	582	n.d.	0.12	n.d.	n.d.	n.a.	n.a.	n.a.
R9a	0	25	2.1	1.35	766	1.23	0.27	0.18	0.09	7.49	829	n.d.
R9b	7	224	101.4	26.31	761	1.00	0.28	0.12	0.08	7.68	346	84
R9c	24	229	156.1	42.72	729	1.16	0.19	0.02	0.02	7.72	n.d.	337
R9d	50	229	152.9	40.42	710	1.05	0.10	0.02	n.d.	7.57	n.d.	306
R9e	169	230	160.3	36.56	687	2.41	0.08	0.02	n.d.	7.58	n.d.	220
R9f	266	230	165.3	34.10	677	2.09	0.11	0.03	n.d.	7.39	n.d.	181
R9g	698	230	131.0	0.10	77	2.71	0.06	0.02	n.d.	5.69	n.d.	47
R9h	1274	227	158.4	0.10	35	3.25	0.01	0.01	n.d.	5.88	n.d.	6
R9i	1706	228	172.9	3.99	38	3.87	0.14	0.04	n.d.	5.60	n.d.	n.d.
R9fin	1716	25	159.4	n.d.	41	2.82	0.07	n.d.	n.d.	5.20	n.a.	n.a.
R11a	0	25	0.0	6.58	407	2.60	0.39	0.10	0.44	2.13	864	n.d.
R11b	3	115	7.8	19.91	405	2.31	0.47	0.14	0.47	2.03	835	n.d.
R11c	6	193	181.0	67.42	400	2.60	0.43	0.19	1.02	2.63	412	26
R11d	24	199	308.7	0.16	393	2.92	0.46	0.11	0.22	3.19	n.d.	60
R11e	50	198	277.6	0.00	390	2.80	0.44	0.10	0.08	3.30	n.d.	66
R11f	151	200	228.8	0.00	372	2.76	0.13	0.04	n.d.	4.16	n.d.	4
R11g	387	200	207.5	0.00	375	4.12	0.44	0.01	n.d.	3.94	n.d.	5
R11h	936	201	158.2	0.25	372	4.14	0.57	0.10	n.d.	3.90	n.d.	2
R13a	0	25	3.4	8.35	390	3.08	0.43	0.13	0.43	1.99	906	n.d.
R13b	3	112	5.9	15.21	390	2.72	0.47	0.13	0.50	1.90	906	n.d.
R13c	8	164	82.7	90.22	380	2.47	0.43	0.13	0.58	2.57	555	30
R13d	26	162	221.2	55.25	380	2.92	0.51	0.13	0.55	2.78	282	39
R13e	48	161	271.1	35.05	350	3.20	0.64	0.15	0.47	2.83	167	46
R13f	72	162	280.0	21.28	345	2.85	0.72	0.16	0.77	2.94	86	58

https://doi.org/10.1346/CCMN.1993.0410208 Published online by Cambridge University Press

Table 2. Continued.

Sample	Time (h)	T°C	Si mg/l	Al mg/l	K mg/l	Na mg/l	Ca mg/l	Mg mg/l	Fe mg/l	pH 25°C	Oxalate mg/l	Formate mg/l
R13g	101	161	286.4	13.81	335	2.81	0.74	0.16	0.81	3.09	95	58
R13h	168	162	295.7	5.68	325	2.95	0.87	0.18	0.73	3.10	23	67
R13i	243	162	300.6	3.18	320	3.35	1.08	0.20	0.62	3.09	14	85
R13j	840	163	184.1	6.12	271	3.77	1.33	0.27	0.37	3.25	n.a.	n.a.
R13fin	850	25	174.3	10.78	240	1.27	1.20	0.21	0.39	3.31	n.a.	n.a.
R14a	0	25	4.0	11.22	441	2.62	0.53	0.12	0.46	2.12	964	n.d.
R14b	3	115	4.9	16.54	352	2.86	0.42	0.12	0.28	1.93	960	n.d.
R14c	8	169	58.3	65.55	377	3.04	0.45	0.12	0.46	2.45	478	58
R14d	24	182	294.3	10.57	339	2.93	0.38	0.12	0.23	2.98	69	106
R14e	32	180	311.9	3.50	419	2.58	0.41	0.10	0.38	3.10	37	107
R14f	49	180	322.6	0.83	407	3.19	0.44	0.12	0.32	3.16	n.d.	89
R14g	96	182	311.9	1.54	409	3.50	0.38	0.12	0.22	3.36	n.d.	46
R14h	123	181	282.1	2.79	366	2.80	0.33	0.10	0.10	3.20	n.d.	44

n.a. = not analysed.
n.d. = not detected.
Samples R..fin are samples recovered after quenching and dismantling the apparatus.

water and was probably an amorphous precipitate formed during quenching of the pressure vessel. In all experiments where the fluid recovered after dismantling the apparatus was analysed, a drop in Si concentration was measured (Table 2). At lower temperature, the kaolinite precipitate is finer grained and is formed of embryonic platelets 0.1 to 0.2 μm diameter (Figure 3b); some larger plates appear to be formed of aggregates of smaller platelets.

Illite precipitation

Illite was formed in five experiments with an initial solution of 0.01 M K-oxalate (R2, R3, R5, R6, and R9). These experiments cover three temperatures; 250°C, 230°C, and 200°C. Pairs of experiments were run at 230°C (R2 and R3) and at 200°C (R5 and R6) with different sampling intervals. R3 and R6 were of shorter duration, examining the early stages of illite precipitation, and in these two experiments fluid composition did not reach a steady state. Air dried XRD patterns of a disaggregated water slurry of post-run gels from the five experiments are shown in Figure 4. Samples from R5 (200°C), R9 (230°C), and R2 (250°C), which are from long duration experiments in which a steady state fluid composition was established, all show reasonably sharp illite 001, 002, and 003 maxima. Glycolation and heating to 550°C produce only a very slight change in 001 peak shape, indicating minor interlayering (<5%) of an expandable component. Samples from R6 (200°C) and R3 (250°C), which were experiments of shorter duration, showed poorly resolved illite basal maxima, and, in the case of R6, the mullite peaks that were present in the starting gel (Figure 2) remain. In R9 hk0 maxima are resolved at 4.33 Å, 4.08 Å, 3.64 Å, and 3.06 Å, indicative of the 1Md mica polytype (Bailey, 1980). A broad, low peak at 12.4°2θ in R9 is likely produced by kaolinite. Synthetic kaolinite formed at 200°C produced sharp, intense 001 peaks (R11, Figure 2); therefore, the diffuse peak at 12.4°2θ in R9 probably represents only a trace amount of kaolinite (<5%).

The morphology of illite precipitated on the sandstone substrate in experiments R2, R3, R5, R6, and R9 was examined by TEM and SEM (Figures 5 and 6). These synthetic illites are characteristically lath-shaped as observed in previous experiments containing aqueous oxalate (Small *et al.*, 1992b). In the 250°C experiments (R2, R3), illite laths were observed in the dispersed TEM samples (Figure 5a), although the *in situ* morphology revealed by SEM (Figure 6a) indicated larger grain-sized particles with a crenulated, platy

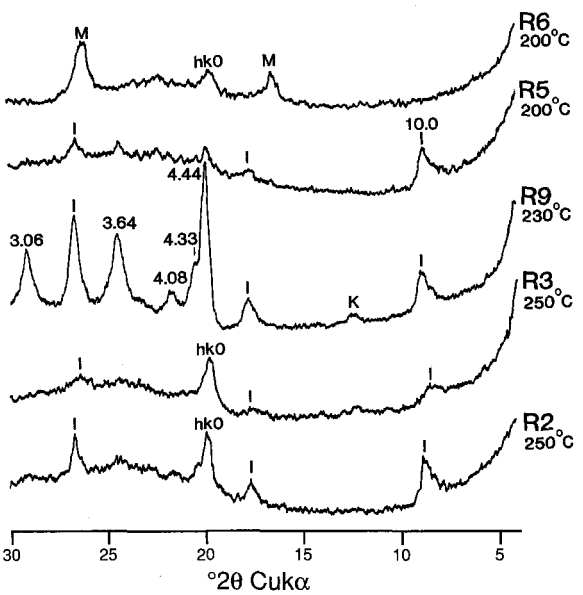

Figure 4. X-ray diffraction patterns (CuKα radiation) of illites formed in experiments R2, R3, R5, R6, and R9. Experiments R3 and R6 were terminated before steady state fluid conditions were established. Specimens are whole samples of post-run gel. I = illite, K = kaolinite, M = mullite, d spacing in Å.

https://doi.org/10.1346/CCMN.1993.0410208 Published online by Cambridge University Press

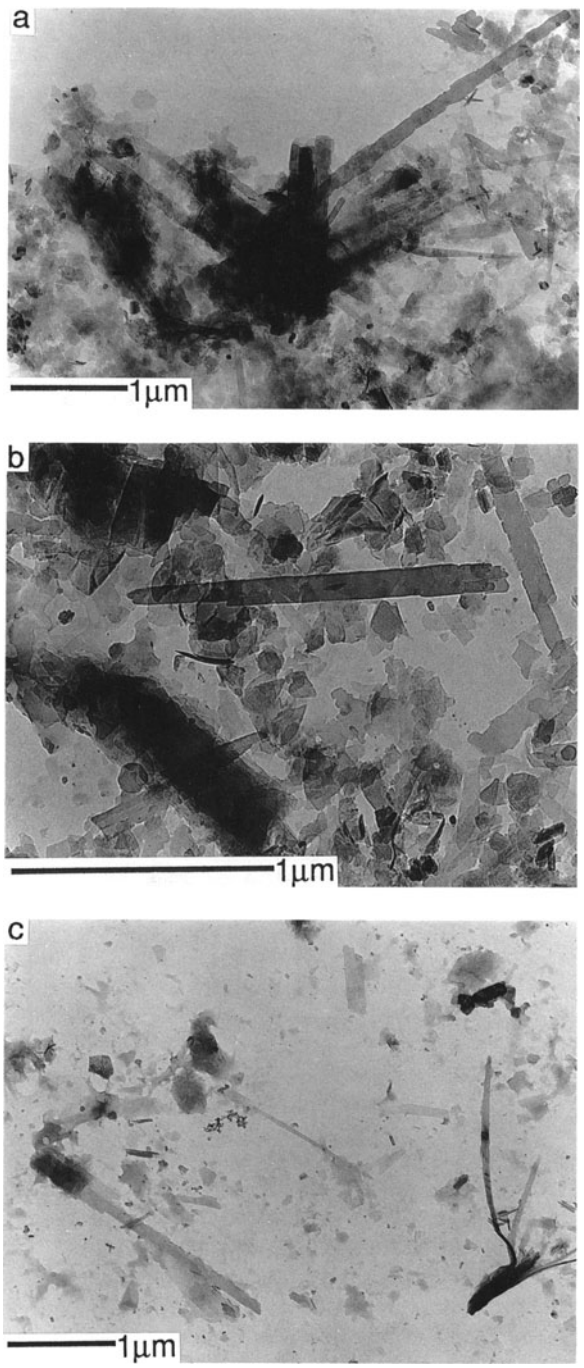

Figure 5. Transmission electron micrographs of dispersed illites precipitated on sandstone cores of experiments: a) R2, 250°C; b) R5, 200°C; and c) R6, 200°C.

morphology. These plates are presumably composed of overlapping laths, a feature observed in authigenic illites formed in sandstones (Macchi, 1987). In the 230°C experiments (R9) (Figure 6b), illite laths had a length/width aspect ratio around 3 to 5 and appeared to be single crystals. Experiments R6 and R5 (200°C) showed that very delicate filaments with aspect ratio >10 are produced initially in R6 after 725 hours (Figures 5c and 6d), which, in R5 after 960 h (Figures 5b and 6c), are wider and form laths with an aspect ratio of around 10.

Experiment R9 showed, in addition to illite precipitation, evidence of quartz dissolution and precipitation. Figure 7 illustrates the complicated nature of quartz dissolution/precipitation, with preferential etching of one crystal face, while other faces on the same crystal may even show new growth. In this example illite also precipitates on the clean crystal face. Minor dissolution of quartz occurs locally in the other experiments, but the enhanced dissolution observed in R9 is at present unexplained.

Average illite structural formulae calculated from ATEM analyses of single, dispersed illite laths from experiments R2, R5, and R6 are given in Table 3, together with comparable ATEM analyses of authigenic illite from sandstones analysed under identical conditions (Warren and Curtis, 1989; Macchi *et al.*, 1990). Interlayer K and tetrahedral Al contents of the synthetic illites are comparable to the Carboniferous Bothamsall illite analysed by Warren and Curtis (1989) and are slightly lower than values reported for Rotliegendes illite and the Irish Sea Triassic illite (Macchi *et al.*, 1990). The Fe content of the synthetic illite is within the range of Irish Sea Triassic illite. The synthetic illite produced in these experiments is, thus, representative of the range of composition of natural authigenic illite in sandstone, which, as noted by Warren and Curtis (1989), is narrow and much more restricted than the range of illite analyses from mudrock samples. Exceptions to this compositional character were noted in R6, which produced very fine, delicate illite crystals in an experiment that was terminated before a steady state fluid composition was attained. In this case, tetrahedral Si contents were higher than natural illites and interlayer K was higher and more variable than in the other synthetic illites. High Si and K synthetic illites were also recorded in previous experiments that did not attain equilibrium (Small *et al.*, 1992b). In these cases, the analyses do not fit the illite formula (tetrahedral Si > 8) and are thought to represent mixtures of illite and a K-silicate phase. On quenching (experiment R6), the fluid composition changed significantly (Table 2), presumably resulting from precipitation during the 8 h required to cool from 200°C to 25°C. The calculated bulk composition of the quench precipitate calculated from the drop in concentration is Si 37 mole%, Al 10 mole%, and K 52 mole% for the final fluid volume of 130 ml, and it is equivalent to a weight of approximately 25 mg expressed as oxides. A coating of this composition on the illite fibres would result in high Si and K analyses. It is likely that the very high K content of the amorphous precipitate would be lowered, either by dissolution during sample preparation or by loss under the electron beam.

https://doi.org/10.1346/CCMN.1993.0410208 Published online by Cambridge University Press

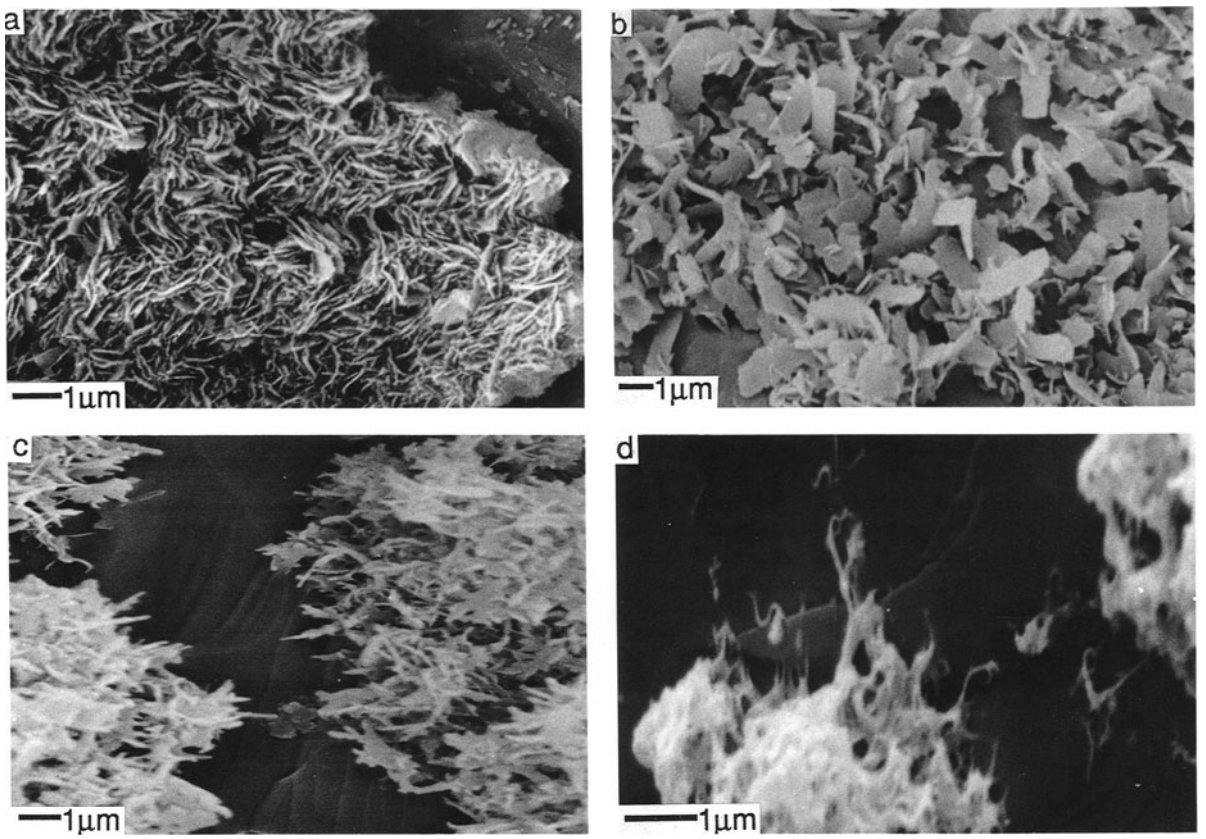

Figure 6. Scanning electron micrographs of illites precipitated on sandstone cores of experiments: a) R2, 250°C; b) R9, 230°C; c) R5, 200°C; and d) R6, 200°C.

Monitoring clay precipitation from fluid analyses

Fluid analyses of samples taken at intervals during the precipitation of illite and kaolinite are listed in Table 2. Figure 8 shows concentration *vs* time plots during illite precipitation at 250°C (R2 and R3); illite experiments at lower temperature produce similar trends over longer time scales. Si concentration (Figure 8a) rose rapidly from close to zero to quartz saturation within the first 24 h, which included heating to 250°C for the first 8 h. Al concentration (Figure 8b) rose at a similar rate to Si during dissolution of the sintered gel, but after 12 h Al concentration declined, which is interpreted to represent precipitation of illite. At 250°C Al concentration reached a steady state after 50 h. K concentration (Figure 8c) also indicates the formation of illite, and steady state conditions are attained after 200 h at 250°C. The slower rate of K decrease compared with that of Al is probably a consequence of illite formation in the gel by localised alteration, i.e., where Al is conserved in the solid phase. For this reason, Al concentration rather than K concentration is used to measure the rate of illite precipitation. Quench pH (Figure 8d) showed a decrease from 7.5 to 6.2 during experiments R2 and R3. The pH change in these experiments was controlled by dissolution and precipitation reactions and the buffering effect of oxalate and its breakdown products formate and carbon dioxide. Na, Ca, Mg, and Fe concentrations (Table 2) in the illite precipitation experiments were all at a trace level but were in most cases above analytical detection. Na

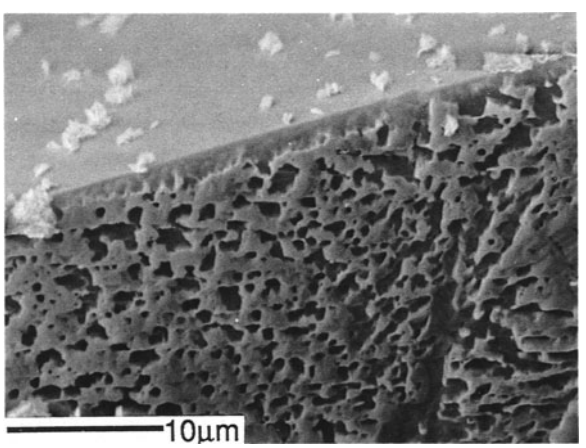

Figure 7. Scanning electron micrographs of an originally fresh quartz overgrowth that has been strongly etched preferentially on one crystal face during experiment R9. Small illite plates and laths are present on the upper, perfect crystal face.

https://doi.org/10.1346/CCMN.1993.0410208 Published online by Cambridge University Press

Table 3. Illite formulae based on 22 oxygens calculated from ATEM analyses of single crystal synthetic and natural authigenic sandstone illites.

Sample	Tet. Si	Tet. Al	Oct. Al	Oct. Fe	Oct. Mg	Int. K	Sum oct.	n
R5								
Mean	6.72	1.28	3.42	0.46	0.06	1.53	3.93	16
σ	0.18	0.19	0.29	0.26	0.08	0.22	0.07	
R6								
Mean	7.32	0.68	3.07	0.47	0.22	1.62	3.76	9
σ	0.18	0.18	0.11	0.06	0.05	0.42	0.10	
R2								
Mean	6.80	1.20	3.54	0.24	0.23	1.38	4.02	6
σ	0.16	0.16	0.27	0.09	0.15	0.20	0.04	
Carb/Bothamsall*								
Mean	6.78	1.22	3.61	0.17	0.25	1.23	4.03	203
σ	0.20	0.20	0.19	0.08	0.12	0.30	0.14	
Rotliegendes*								
Mean	6.61	1.39	3.38	0.25	0.31	1.88	3.93	58
σ	0.15	1.00	0.15	0.07	0.07	0.16	0.05	
Trias/Irish sea**								
Mean	6.56	1.44	3.23	0.42	0.39	1.67	4.05	

* Warren and Curtis (1989).
** Macchi *et al.* (1990).
Note: Natural illite analyses * and ** contain up to 0.1 interlayer Na + Ca atoms not included above.

and Ca ranged up to 4 mg/l and 0.3 mg/l, respectively, and behaved independently of K; Na and Ca were not identified as interlayer cations by ATEM. Fe and Mg are incorporated into the precipitated illite (Table 3) and measured Fe and Mg fluid concentrations decrease with time from a maximum of 0.2 mg/l.

Fluid concentration data from experiment R14 (180°C) during kaolinite precipitation are illustrated in Figure 9. Si and Al concentrations (Figures 9a and 9b) indicated rapid dissolution during the first 24 h. Al concentration then fell as kaolinite precipitated and attained a steady state after 50 h. Si concentration greatly

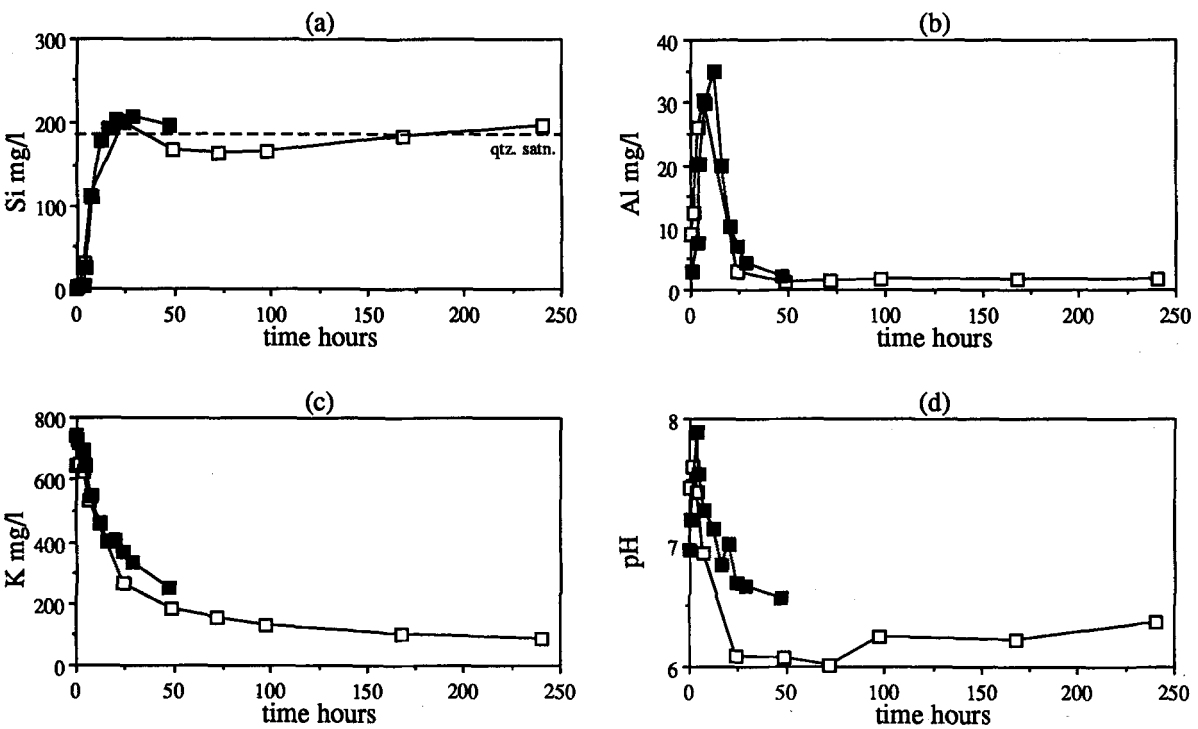

Figure 8. Plots of solute concentration *vs* time for illite precipitation experiments R2 (open symbols) and R3 (closed symbols), 250°C.

https://doi.org/10.1346/CCMN.1993.0410208 Published online by Cambridge University Press

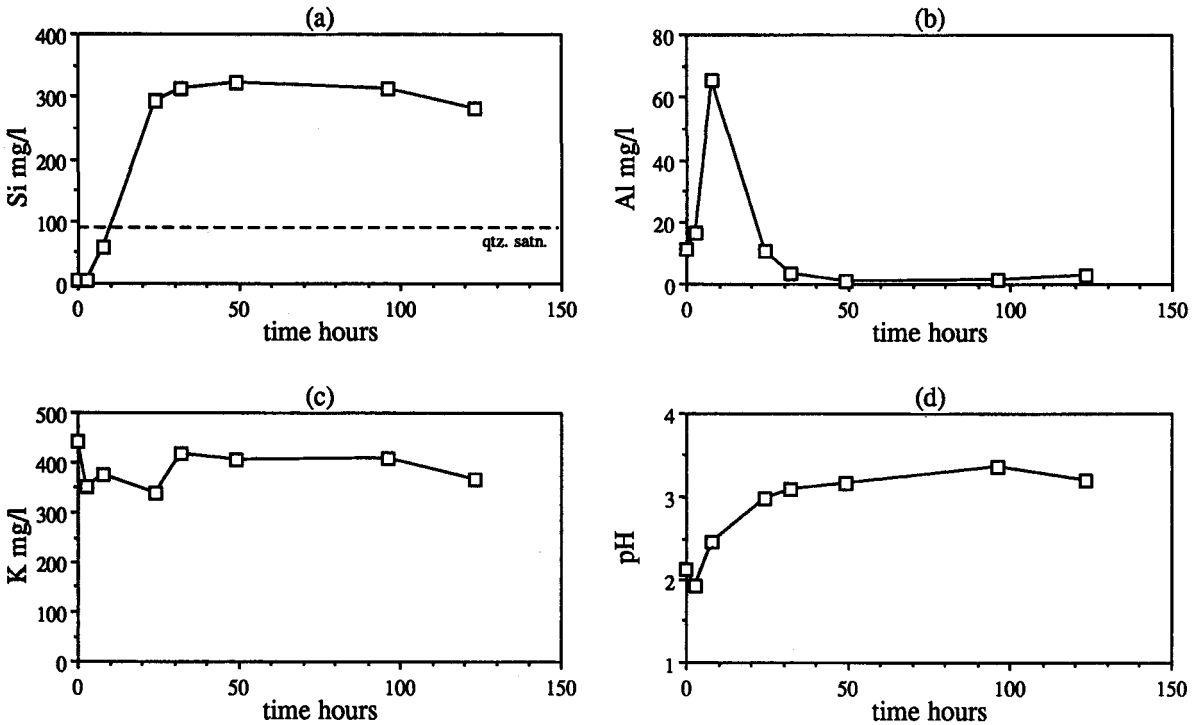

Figure 9. Plots of solute concentration *vs* time for kaolinite precipitation experiment R1, 180°C.

exceeded quartz saturation but declined towards saturation in experiments R11 and R13, which are of longer duration than R14 (Table 2). An experiment under similar fluid conditions at 250°C, but with the inclusion of a sandstone substrate (Small and Manning, 1993), also produced oversaturated conditions with respect to quartz, suggesting that nucleation of quartz is not limiting Si precipitation. K concentration (Figure 9c) remained constant during experiments R11 and R14; however, in R13 (160°C) there was a significant decrease of 120 mg/l K during the experiment (Table 2). The first 45 mg/l K was lost when Al concentration declined, while the final drop of 75 mg/l was associated with a slight increase in Al concentration and a change in Si concentration from 300 to 184 mg/l. A further 30 mg/l K and 10 mg/l Si was lost on quenching the experiment. Considering the similar precipitation effects during quenching of R6 and the occurrence of apparently K-rich and Si-rich synthetic illites (Small *et al.*, 1992b), it appears that K-silicate phases can form in this type of experiment at temperatures <200°C from solutions oversaturated with respect to quartz. This probably accounts for the significant drop in K concentration in experiment R13. It is not known whether such a phase also contains any significant amount of Al.

Effect of oxalate on clay precipitation

In all clay precipitation experiments oxalate concentrations (Table 2) decreased from the initial 0.01 M concentration (880 mg/l) to below detection (<1 mg/l). Formate was detected as a breakdown product of oxalate, and a gaseous phase was exsolved from the fluid on sampling but was not analysed in these experiments. Results presented in Small (1993) show that gas produced during oxalic acid decomposition in the same apparatus is composed of CO_2 and H_2 with trace quantities of C_1-C_3 hydrocarbons. Figure 10 compares the timing of oxalate decomposition and the precipitation of kaolinite (monitored by Al concentration) at 160°C (R13). The two sets of data coincide point for point, indicating that the rate of oxalate decomposition was the same as the rate of Al decrease. A similar relationship occurred in the other kaolinite experi-

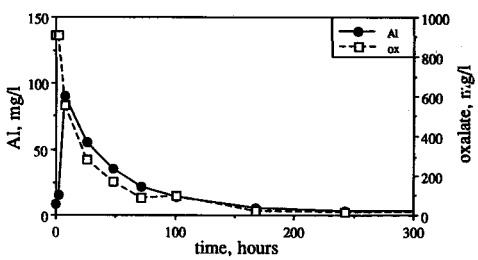

Figure 10. Comparison of the decrease in oxalate concentration during oxalate decomposition with the decrease in Al concentration during the precipitation of kaolinite, 160°C. The coincidence of the two sets of data suggests that kaolinite precipitation is rate limited by the decomposition of oxalate.

https://doi.org/10.1346/CCMN.1993.0410208 Published online by Cambridge University Press

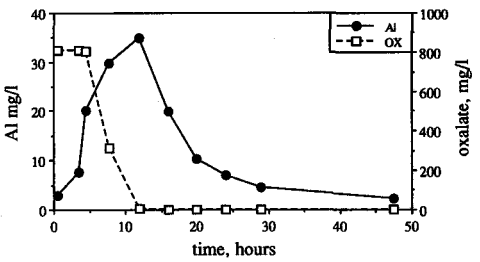

Figure 11. Comparison of the decrease in oxalate concentration during oxalate decomposition with the decrease in Al concentration during the precipitation of illite, 250°C.

ments (R11 and R14). This suggests that the rate limiting step in the precipitation of kaolinite in these experiments is the breakdown of oxalate. Implications for Al-oxalate complexing from this data are discussed in Small (1992, 1993).

Figure 11 compares the rate of oxalate decomposition with the rate of decrease in Al concentration in illite precipitation experiment R3. The rate of illite precipitation was significantly slower than the rate of oxalate decomposition. This suggests that for illite precipitation oxalate decomposition was not rate limiting. Aqueous speciation modeling using EQ3/6 indicates that illite precipitation is controlled by pH variation, which is in turn controlled by oxalate decomposition (Small, 1992, 1993).

Relevance of experimental results to diagenesis

Before these experimental results can be applied to diagenesis, it is vital to consider whether the precipitation reactions studied at high temperature are representative of those occurring during diagenesis. The main evidence supporting these results is the morphological and compositional similarity of the synthetic clay minerals to natural authigenic equivalents. For illite, the experiments reproduce both the fibrous/lath morphology of authigenic illites in sandstones and the narrow composition range. Chermak and Rimstidt (1990) have shown that the rate of illitization of kaolinite is increased by the presence of metallic iron. The present experiments contain aqueous Fe, probably buffered by hematite and ferric hydroxides present on the sandstone core. As the Fe content of the synthetic illite is similar to authigenic illite in sandstones, any effect of Fe on the illite precipitation rate should be geologically reasonable. The morphology of synthetic illite appears to be controlled by precipitation rate; fibrous illite being formed from highly oversaturated fluids (with high Al concentrations) when precipitation rate is higher, while platy illite forms at lower rates (Small *et al.*, 1992b; Small and Manning, 1993). This observation is supported by results from experiments R5 and R6 (Figures 5b, 5c, 6c, and 6d) which show that the first illite to form is filamentous (R6) while later-formed illite is wider and lath-like (R5). Assuming that illite morphology is related to precipitation rate and that reaction rate is proportional to the degree of oversaturation (Q/K) (Lasaga, 1984), the initial high saturation produced from dissolution of Al/Si gel in K-oxalate should be realistic of conditions during diagenesis that form authigenic fibrous illite in sandstones. It is important that dissolution and precipitation rates are measured at appropriate saturation since rates of reaction may not always be linearly dependent on Q/K (Nagy *et al.*, 1991).

Synthetic kaolinite produced in the presence of oxalate has a tabular, hexagonal morphology, which is perhaps most closely representative of blocky kaolinite, characteristic of late-stage growth in sandstones (Glasmann *et al.*, 1989b; Ehrenberg, 1991). Vermicular kaolinite, characteristic of early formed authigenic kaolinite from meteoric derived fluids (Glasmann *et al.*, 1989b), has been synthesised by hydrochloric acid dissolution of albite (Small *et al.*, 1992a). This variation in kaolinite morphology could reflect different precipitation mechanisms controlled by inorganic or organic aqueous species. Trace amounts of Al-oxyhydroxide phases are present in the lowest temperature experiment (R13), which occur metastably under the measured fluid conditions. Their presence may indicate that the tabular kaolinite morphology results from the initial precipitation of Al-oxyhydroxides, which are subsequently transformed into kaolinite by the incorporation of silica. The implication of this is that the rate of decrease in Al concentration reflects the rate of precipitation of a precursor Al-oxyhydroxide rather than the rate of formation of kaolinite, which is a more complex and, overall, a slower process. Aluminium is considered to be the critical component in aluminosilicate mass-transfer calculations (Lasaga, 1984) thus it is valid to use the measured rate of Al decrease, which leads to the formation of kaolinite as a limiting control on kaolinite formation. Rates of kaolinite precipitation derived from these experiments should not necessarily be applied to the formation of vermicular kaolinite, which may well form by a different mechanism.

Measurement of precipitation rate

Rates of precipitation of illite and kaolinite are measured by the rate of decrease in Al concentration following the initial period of dissolution of the Al/Si gel (Figures 8b and 9b and Table 2). Al concentration *vs* time data are fitted to the integrated first order rate equation;

$$(C_t - C_e)/(C_o - C_e) = e^{-k't} \quad (1)$$

where C_t is the concentration at time t, C_o is the initial concentration, C_e is the steady state (equilibrium) concentration, and k′ is the apparent first order rate constant. The point of maximum Al concentration (Figures 8b and 9b) is assumed to represent time = 0. For heterogeneous reactions between fluid and solid phases the measured apparent rate constant, k′, is dependent

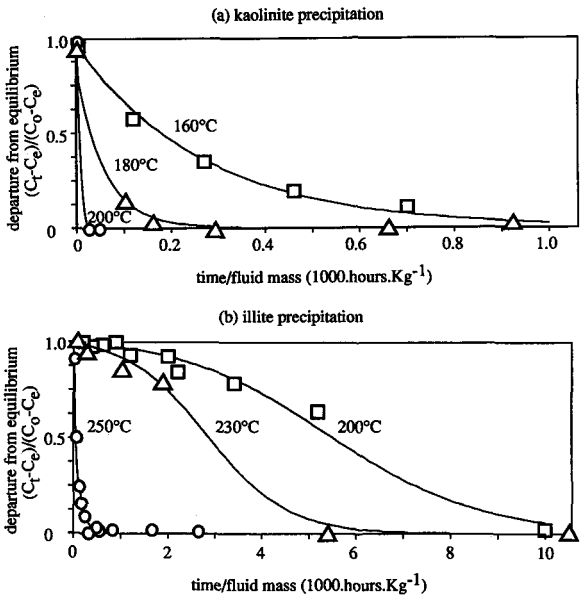

Figure 12. Normalised Al concentration *vs* reaction time/fluid mass for a) kaolinite precipitation experiments and b) illite precipitation experiments. Curves plotted are produced from a curve fitting procedure (see text).

on the reactive surface area (A) and the mass of solution (M) (Rimstidt and Barnes, 1980). It is, at present, not possible to quantify the active surface area available for clay precipitation; therefore, the total surface area is used, assuming that the reactive area is proportional to the total area for a particular mineral. The apparent rate constant (k′) is normalised to a standard reference state (k), where A = 1 m² and M = 1 kg and equation 1 becomes;

$$(C_t - C_e)/(C_o - C_e) = e^{-kt(A/M)} \qquad (2)$$

In the Dickson fluid sampling apparatus the mass of solution (M) decreases with time as samples are removed during the experiment. In order to evaluate k where M is changing with time, the rate of change of Al concentration must be compared as a function of t/M. Figure 12 shows Al concentration data for kaolinite and illite precipitation experiments plotted against t/M. For each sampling point M is taken as the fluid mass of the reaction cell in the time interval between the last sampling.

The amount of kaolinite and illite precipitated in the experiments (expressed as a percentage of the weight of the starting gel, 1 g) can be estimated from the decrease in Al concentration and is around 40% for illite and 25% for kaolinite. This substantial amount of precipitate is likely to alter the total surface area of the experiment. The initial total surface area of the sintered gel is 0.4 m²/g. Surface areas of post-run samples measured by the BET method are quite variable between experiments and are in the range 20 to 200 m²/g. The high and variable surface areas measured are probably

Table 4. Apparent precipitation rate constants (k′, hr^{-1}), surface area coefficients, and correlation coefficients from curve fitting and standardised rate constants: (log(k), s^{-1}) for A/M = 1 m²/Kg.

T°C	k′	CSA	SAo	r²	log(k)
Kaolinite					
200	7.02	0.0	1.0	(2 point ts)	−6.71
180	0.73	0.0	2.3	0.9854	−7.33
160	0.36	0.0	1.0	0.9949	−8.00
Illite					
250	0.98	0.0	1.3	0.9911	−7.45
230	0.108	1.1	0.04	0.9912	−8.47
200	0.098	0.6	0.02	0.9805	−8.77

a consequence of the precipitation of amorphous silica during the slow quenching of the Dickson vessel following termination of the experiment. This precipitate is inferred from a decrease in aqueous silica concentration between the final *in situ* fluid sample and a sample after quenching (Table 2). The measured surface areas of experimental products are, therefore, meaningless in regard to the active surface area during clay precipitation. To account for a possible effect of increased surface area during clay precipitation, the data in Figure 12 are fitted to Eq. 2 by a least squares algorithm. This increases the surface area A in direct proportion to the normalised concentration of Al precipitated (C_{Al}, equal to $C_o - C_t/C_o - C_e$);

$$A = (C_{Al} \cdot CSA + SAo) \qquad (3)$$

where SAo is a coefficient proportional to the initial surface area and CSA is a coefficient proportional to the additional surface area produced as Al precipitates. CSA, SAo, and an apparent rate constant k′ are determined by the best fit algorithm. This routine can also be used to fit first order rate data to systems where active surface area does not increase during precipitation (CSA = 0). Best fit curves are plotted on Figure 12; best fit coefficients (CSA and SAo), correlation coefficients (r^2) and apparent rate constants (k′) of experiments are given in Table 4.

For the kaolinite precipitation experiments (Figure 12a), the concentration data decrease exponentially with t/M, and the best fit curves all have coefficient CSA = 0. This indicates that the kaolinite precipitation reaction is first order with respect to Al concentration and that the active surface area does not increase as kaolinite precipitates. For illite precipitation (Figure 12b), the data for the 250°C experiment also follow an exponential decrease in concentration with t/M and CSA = 0. For illite precipitation at 230°C and 200°C, Al precipitation rate is initially slow, but later the rate increases and the curve takes on an exponential form. The 200°C and 230°C data can be reasonably fitted by curves where CSA is greater than 0, i.e., where the active area for illite precipitation increases as illite forms. This control of precipitation rate by surface area

https://doi.org/10.1346/CCMN.1993.0410208 Published online by Cambridge University Press

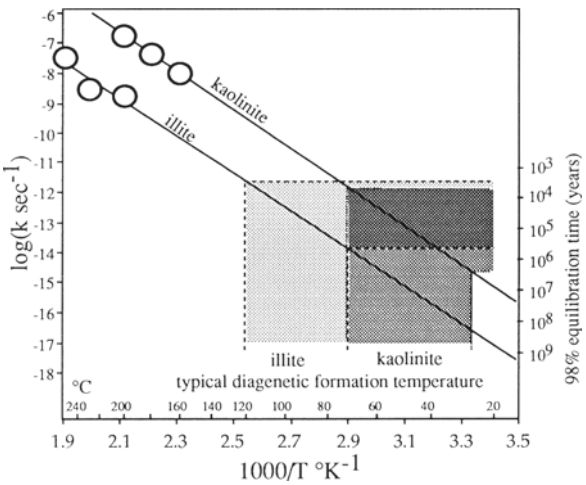

Figure 13. Arrhenius plot of log(k) for illite and kaolinite precipitation and extrapolation of best fit lines to diagenetic formation temperatures.

is considered to be a nucleation effect. The reasonable fit of Eq. 2 to the Al concentration data ($r^2 > 0.98$) indicates that both illite and kaolinite precipitation can be considered first order at constant active surface area and fluid mass.

Rate constants (k) normalised to a standard state of A = 1 m² and M = 1 kg fluid are obtained from the best fit value of k′, CSA, and SAo, assuming that the final surface area of the experimental system is 10 m², based on an assumed final mineral specific surface area of 10 m²/g. For the illite experiments, where active surface area apparently increases during precipitation, the final surface area (A_{final}) can be calculated in proportion to the initial surface area ($A_{initial}$, measured by the BET method) using;

$$A_{final} = CSA \cdot A_{initial}/SAo \quad (4)$$

The 200°C and 230°C experiments have A_{final} values calculated in this way of 12.4 m² and 11.4 m², respectively, which are in good agreement with the assumed surface area of 10 m². This independent estimate of final surface area assumes that the initial sintered gel and the precipitated illite have the same number of growth sites per unit surface area.

Temperature dependence of precipitation rate

Rate constants (k s^{-1}) for illite and kaolinite precipitation between 160°C and 250°C are plotted on the Arrhenius diagram (Figure 13). The top and bottom of the symbols represent log(k) calculated assuming final surface areas ranging from 5 m² to 20 m², respectively, and give an indication of the error introduced by assuming a value for active surface area. For the experimental conditions used, the rate of kaolinite precipitation is 2 orders of magnitude greater than that of illite. The log(k) values for both illite and kaolinite show a linear Arrhenius relationship with 1/°K and the best fit lines plotted (Figure 13) have the following equations:

Table 5. Activation energies for illite and kaolinite precipitation and comparable values for illite and kaolinite formation by different mechanisms from previous studies.

Reaction	Ea (kJ·mol^{-1})
Kaolinite ppt from solution (this study)	124
Illite ppt from solution (this study)	110
Smectite to illite in I/S	
(Eberl and Hower, 1976)	82 ± 15
(Robertson and Lahann, 1980)	126 ± 21
(Huang *et al.*, 1991)	24
Kaolinite to muscovite (Chermak and Rimstidt, 1990)	155 ± 15
Muscovite to kaolinite (Chermak and Rimstidt, 1990)	101 ± 10
Kaolinite synthesis from gels (Huertas *et al.*, 1991)	110 (mean)

Illite $\log k = -6.25 \times 10^{-3} 1/T + 4.26$

$R^2 = 0.825 \quad (5)$

Kaolinite $\log k = -6.45 \times 10^{-3} 1/T + 6.17$

$R^2 = 0.999. \quad (6)$

The slope of these equations is equal to −Ea/(2.303R), where R is the gas constant and Ea is the activation energy. Values of Ea for illite and kaolinite precipitation in this study are similar to those previously determined for illite and kaolinite formation (Table 5). This indicates that the slope of the Arrhenius relationship used to extrapolate log(k) to lower temperatures is reasonable.

Extrapolation of the Arrhenius relationships to typically estimated temperatures of occurrence of authigenic illite and kaolinite in sandstone reservoirs (Glasmann *et al.*, 1989a, 1989b; Scotchman *et al.*, 1989; Lee *et al.*, 1989), and correction to A/M ratio of 20 m²/Kg appropriate for sandstones (see later) predicts that illite and kaolinite precipitation would require between 5 × 10^3 and 5 × 10^6 years to approach equilibrium. For illite, estimated precipitation times are in accord with measured K/Ar ages (see later). These geologically sensible precipitation times suggest that the mechanism of precipitation in these experiments is the same as that occurring during diagenesis.

MODELING CLAY PRECIPITATION RATE DURING BURIAL

The formation of authigenic clays in sandstones is controlled by the stability of minerals in various pore fluids, the rates of mineral dissolution and precipitation, and the rates of transport of solutes in pore fluid. A specific clay mineral can precipitate provided that: 1) the clay mineral is stable or metastable at the pressure, temperature, and fluid composition; and 2) the

https://doi.org/10.1346/CCMN.1993.0410208 Published online by Cambridge University Press

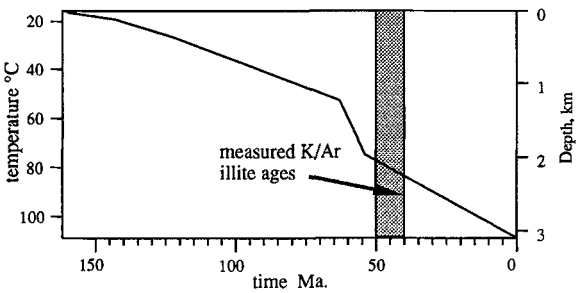

Figure 14. Burial curve of Brent Sandstone in N.W. Hutton Crest Well, 211/27-3, from Scotchman *et al.* (1989). This curve was used to calculate temperature history for modeling illite and kaolinite precipitation (Figures 15 and 16).

rate of precipitation of the clay mineral is sufficiently fast over the geological time scale. The distribution of the clay mineral will depend on the relative rates of precipitation and solute transport. The formation of an authigenic clay mineral may effectively be controlled by any one of these factors. The present results can be used to estimate the rates of precipitation of illite and kaolinite in a sandstone as it is progressively buried and to assess whether precipitation rate is a controlling influence on their formation. The illite and kaolinite precipitation experiments carried out examine only a single set of chemical conditions for each mineral and are a first step into the investigation. The conditions are, however, generally applicable to clay formation in sandstones from pore fluids with unstable dissolved organic acid anions.

The model is based on the experimental Arrhenius relationships defined in Figure 13 and Eqs. 5 and 6, which are used to calculate rates of precipitation at temperatures along the burial curve of a sandstone (Figure 14). In the examples shown, a geothermal gradient of 30°C/km and a surface temperature of 15°C are used to calculate temperatures at 0.1 Ma increments. Since the rate of precipitation is dependent on the reactive surface area and fluid mass (Eq. 2), the standard state rate constant (k) has to be corrected to an appropriate A/M for a sandstone. Rimstidt and Barnes (1980) provide an equation to calculate A/M for an idealised sandstone composed of close packed spheres of uniform radius; calculated A/M values for sandstones with grain radii of 1 mm and 0.1 mm are 8.55 m^2/Kg and 85.5 m^2/Kg, respectively. An alternative calculation based on a measured BET surface area of 0.02 m^2/g for a 150–250 μm quartz sand (Dove and Crerar, 1990) and assuming 10% porosity gives an A/M value of 50 m^2/Kg. Considering these estimates, an A/M value of 20 m^2/Kg was chosen to model precipitation within a sandstone. The model adopts a simplified approach where an oversaturated fluid is instantaneously flushed into the sandstone. The normalised concentration of Al in the sandstone pore fluid is then calculated, as illite or kaolinite precipitates, at intervals during burial using:

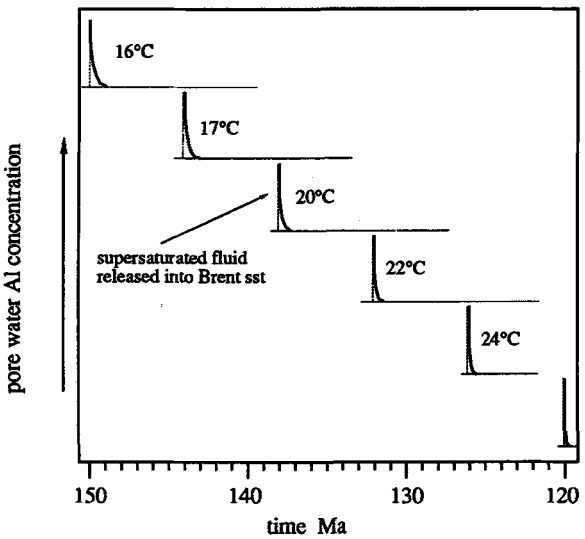

Figure 15. Predicted kaolinite precipitation between 150 and 120 Ma B.P. in the Brent Sandstone of N.W. Hutton Crest (Figure 14). Curves represent the modeled decline in Al concentration as kaolinite precipitates following instantaneous injection of a kaolinite oversaturated fluid at intervals during the burial history of the sandstone. The initial temperature of the fluid is given next to each curve.

$$C_{t-\Delta t} = C_t \cdot e^{(-k_t \cdot \Delta t)} \quad (7)$$

where C is the Al concentration at time t, k_t is the calculated rate constant for that interval temperature and Δt is the time step (0.1 Ma). This algorithm results in a profile of decreasing pore water Al concentration with time (Figures 15 and 16). The predicted timing of clay precipitation is defined by the interval of decrease in pore water Al concentration and can be compared to the actual timing of clay formation estimated from petrographic, K/Ar, and oxygen isotope studies. A convenient measure of precipitation time is the time required for the Al concentration of the initial oversaturated fluid to fall by 98% of that required to reach equilibrium. Figure 17 shows how predicted illite precipitation time varies with burial history for a series of North Sea examples in which authigenic illites have been dated by the K/Ar method.

Case studies

Figures 15 and 16 show examples of kaolinite and illite precipitation modeling for the published burial curve (Figure 14) of the Brent sandstone in the North Sea East Shetland Basin well 211/27-3 situated on the crest of the N.W. Hutton fault block (Scotchman *et al.*, 1989). The model predicts that kaolinite would precipitate instantaneously (<1 Ma) compared with the 160 Ma burial history; predicted times to reach 98% equilibration during kaolinite formation are between 1 Ma and 0.3 Ma at 15°C and 30°C (Figure 15). These results indicate that kaolinite precipitation is unlikely

https://doi.org/10.1346/CCMN.1993.0410208 Published online by Cambridge University Press

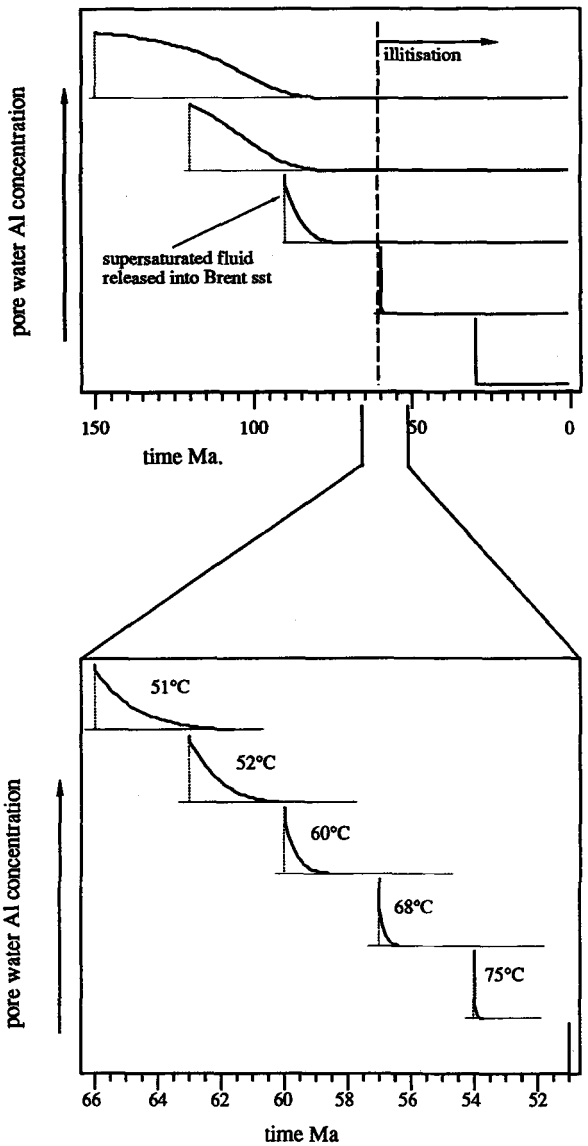

Figure 16. Predicted illite precipitation during burial of Brent Sandstone in the N.W. Hutton Crest (Figure 14). See Figure 15 for explanation of curves. Lower set of curves show, at a higher resolution, the time required to precipitate an illite oversaturated fluid at a temperature of around 60°C, which corresponds to the observed illitization threshold in northern North Sea sequences.

to be kinetically controlled and that kaolinite should form at all stages of burial diagenesis provided that it is chemically stable.

Illite precipitation in the N.W. Hutton well (Figure 16) is predicted to occur at a much slower rate than that of kaolinite and a hypothetical illite oversaturated fluid present at deposition would take over 50 Ma to precipitate. For a fluid released at 60 Ma and 60°C equilibrium would be approached in around 1.4 Ma (Figure 17a). Illite cementation of the N.W. Hutton Brent Group reservoirs has been described by Scotchman *et al.* (1989) and dated using K/Ar methods by Cocker *et al.* (1988). Illites formed between 39 Ma and 49 Ma and have average ages of 41 Ma for the water zone and 43.1 Ma for the oil zone. The water zone samples have a very narrow age range of 40.4 to 41.3 Ma, suggesting that illite precipitation was a short-lived event. The predicted illite precipitation time for the Brent Sandstone at 40–50 Ma is between 0.1 and 0.2 Ma (Figure 17a) and occurs at temperatures of around 80°C. A similar narrow range of illite ages between 166 Ma and 178 Ma at an estimated formation temperature of 88°C have been recorded by Lee *et al.* (1989) for the southern North Sea Leman gas field. Such narrow ranges of K/Ar illite ages are consistent with the rapid precipitation times predicted at 80°–90°C. In other northern North Sea sequences in the East Shetland Basin, well-resolved K/Ar illite age *vs* depth profiles of around 30–50 Ma have been reported in which measured age at any one depth has a range of around 5 Ma, but where age progressively changes with depth (Hamilton *et al.*, 1989). These age profiles have been interpreted to represent processes such as progressive filling of reservoirs (Glasmann *et al.*, 1989b), or progressive illitization (Hogg *et al.*, 1991). Modeling of these burial sequences predicts rapid illite precipitation times (<0.1 Ma) similar to the N.W. Hutton example. Interpretation of age/depth profiles for the 30–50 Ma northern North Sea event as resulting from timing of authigenic illite growth are, therefore, feasible in terms of the predicted rate of illite precipitation. In practice, resolution of K/Ar age profiles will be decreased by analytical error and contamination by detrital K-feldspar and mica (Hamilton *et al.*, 1989).

Lee *et al.* (1989) have constrained illite formation and hydrocarbon migration in the Groningen Field well G1, where gas-zone <0.1 μm illite has an age of 151 Ma, and water zone <0.1 μm illite has an age of 120 Ma. Modeled illitization of well G1 (Figure 17b) shows that during this period illite would take between 0.5 and 3 Ma to precipitate. Note that in this example predicted equilibration time increases with younger age as this period of illitization is associated with uplift. Lee *et al.* (1989) recognised that the age of the finest illite fraction (normally <0.1 μm) marks cessation of illite precipitation since it is composed of the most recently formed material. The finest possible illite fraction is also used for K/Ar dating because it is likely to represent the purest authigenic illite; coarser size fractions are likely to contain reworked mica and K-feldspar, which will give apparently older ages (Hamilton *et al.*, 1989). In most cases in which reported K/Ar ages represent the cessation of illite precipitation, less emphasis has been placed on the older ages recorded. Burley and Flisch (1989) for the Tartan Field and Glasmann *et al.* (1989a) for the Huldra field record illite ages that they interpret with the aid of detailed petrography to represent the initiation of illite authigenesis. For the Tartan Field illitization in the oil-zone

https://doi.org/10.1346/CCMN.1993.0410208 Published online by Cambridge University Press

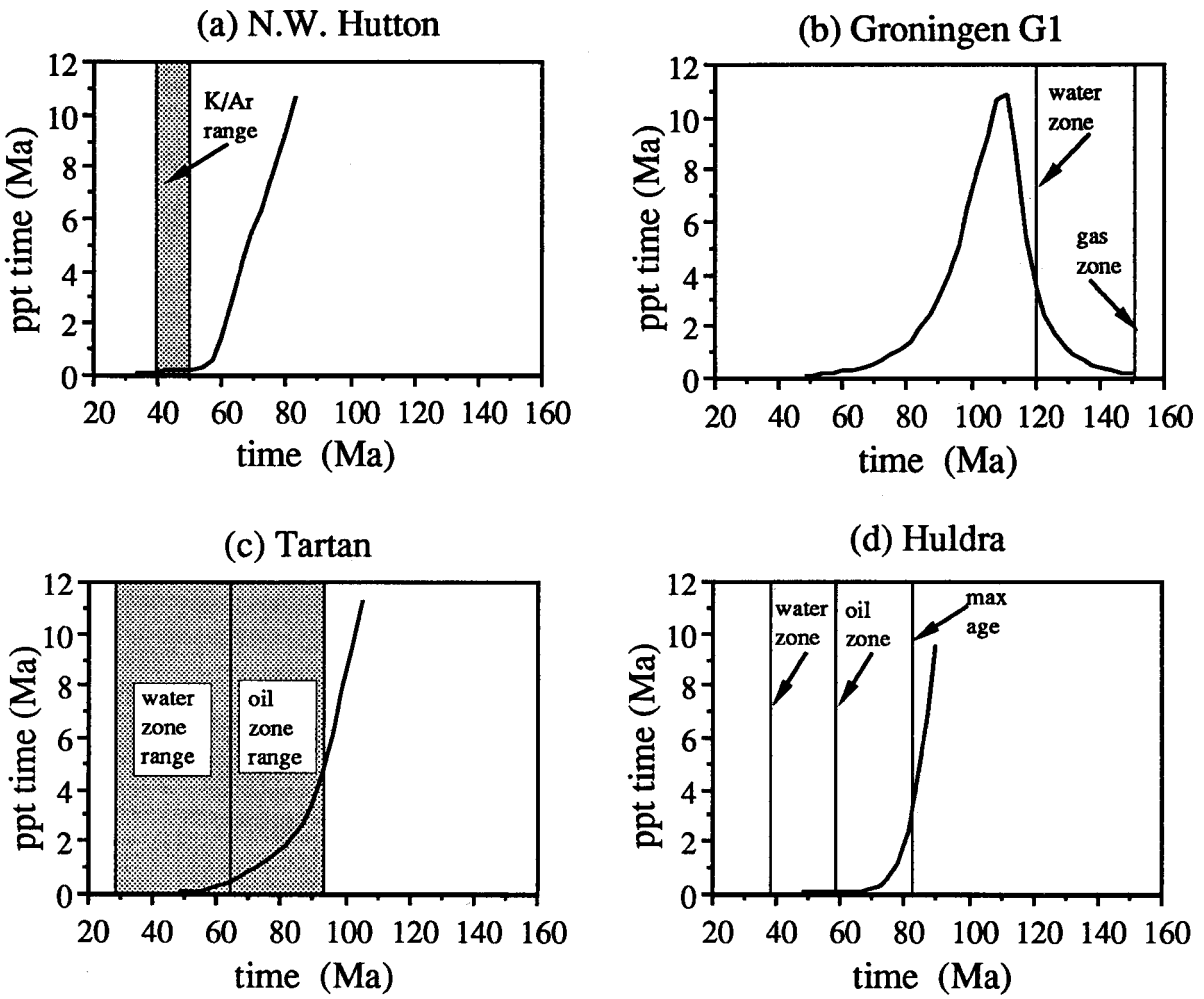

Figure 17. Predicted illite precipitation times (time required for Al concentration of illite oversaturated fluid to reach 98% approach to equilibrium) during burial history of four North Sea well sequences with K/Ar dated authigenic sandstone illites: a) Brent Sandstone in N.W. Hutton Crest well 211/27-3 (Scotchman *et al.*, 1989); b) Rotliegendes Sandstone in Groningen Gas Field well G1 (Lee *et al.*, 1989); c) Piper Sandstone in Tartan Field downthrown block (Burley and Flisch, 1989); and d) Brent Sandstone in Huldra field well 30/2-1 (Glasmann *et al.*, 1989a).

is considered to start sometime between 90 Ma and 65 Ma (Burley and Flisch, 1989). Modeling (Figure 17c) predicts that at this time interval illite precipitation would require between 3 and 1 Ma to approach equilibrium. The earliest date from the Huldra Field, obtained from a 2–15 mm illite fraction in which there is no apparent detrital contamination (Glasmann *et al.*, 1989a), is 83 Ma; predicted illite precipitation time at this time is around 2 Ma (Figure 17d).

The predicted precipitation time of 2 to 3 Ma at the initiation of illite authigenesis in the Tartan and Huldra fields is the same as that for the cessation of illite precipitation in the uplifted Rotliegendes well G1. This is interpreted to represent a kinetic threshold that controls illite formation by the relative rates of precipitation and fluid flow rate. Giles (1987) has reviewed estimates of groundwater flow rates; compaction-driven flow ranges between 10^{-7} and 10^{-3} my, while convectional driven flow in aquifers is between 10^{-1} and 10^{3} my^{-1}. Very high flow rates (>10 my^{-1}) are characteristic of unconfined flow in aquifers and of flow in active hydrothermal systems. Assuming a compaction driven flow rate of 10^{-5} my^{-1}, characteristic of deep burial (Giles, 1987), and an illite precipitation time of 2 Ma, illite would precipitate in a zone up to 20 m away from the solute source; for a flow rate of 10^{-4} my^{-1}, the zone would extend to 200 m. Even with these most modest flow rates, illite-oversaturated fluids released before the 2 Ma precipitation time threshold would be distributed so widely as to be probably insignificant. A precipitation time of 2 Ma seems a reasonable kinetic threshold for the initiation of illite precipitation in consideration of compaction flow rates and is in good agreement with the observed illitization

https://doi.org/10.1346/CCMN.1993.0410208 Published online by Cambridge University Press

of the North Sea wells studied. After this threshold, illite precipitation can be considered kinetically feasible and will be controlled by the supply of illite saturated fluids.

Considering higher aquifer flow rates such as 1 my^{-1} for a thermally driven convection within a 100 m thick homogeneous sandstone with 25% porosity (calculated by Wood and Hewlett, 1982) predicted illite precipitation at around 60°C would extend to a distance of over 1000 km. Precipitation times of ~100 years would be required to restrict illite precipitation to a 100 m zone, which is equivalent to a temperature of 160°C. This suggests that illite precipitation during diagenesis is kinetically feasible only at slow, compaction-driven flow rates.

SUMMARY

The temperature dependence of the rates of precipitation of illite and kaolinite has been determined from the rate of decrease of aqueous Al concentration. Precipitation rate has been determined in solutions initially containing 880 mg/l oxalate, which decomposes during the experiment to concentrations at or below oxalate concentrations in natural pore fluids. The breakdown of oxalate acts as a solubility control over illite and kaolinite precipitation. Kaolinite precipitation is effectively rate limited by oxalate breakdown, while illite precipitation is a considerably slower process controlled by nucleation and crystal growth.

The morphology and composition of the precipitated illite and kaolinite is realistic of authigenic clays formed in sandstones. The extrapolated rates of precipitation of illite and kaolinite are also consistent with the temperature/time of formation of these clays during burial. This evidence provides good support for use of these experiments as analogues of aluminosilicate dissolution/precipitation in oil field pore waters, containing unstable dissolved carboxylic acid anions that may exhibit a transient control over mineral solubilities.

Applying the measured rate of illite precipitation to case burial histories where the timing of illitization is constrained by K/Ar dating suggests that authigenic illite formation in sandstones is kinetically controlled. Below a minimum temperature threshold of around 60°C for northern North Sea well sequences, illite precipitation rate is too slow relative to likely rates of fluid movement for any detectable amount of illite to be precipitated. This threshold corresponds to a precipitation time of around 2 Ma. Illites formed after this threshold, such as the 30–50 Ma North Sea Brent Sandstone illites, will be controlled hydrologically by tectonic and geothermal events. The predicted precipitation time of this main phase of northern North Sea illitization is around 0.1 Ma and meaningful interpretation of high resolution (1 Ma) illite K/Ar age *vs* depth profiles should be feasible. Comparison of predicted illite precipitation times with groundwater flow rates suggests that significant illite precipitation would only occur under slow, compaction-driven fluid flow conditions.

ACKNOWLEDGMENTS

This research has been supported by grants from the Natural Environment Research Council to C. D. Curtis (D1/G1/189) and to D. A. C. Manning (GR3/6141 and GST/02/157) and a British Petroleum extramural research award to D. A. C. Manning and C. D. Curtis. The manuscript was improved after reviews by Laura Crossey, Paul Lundegard, and Reed Glasmann. I am most grateful to David Manning for his advice in the operation of the experimental equipment and for our helpful discussions.

REFERENCES

Aja, S. U., Rosenberg, P. E., and Kittrick, J. A. (1991) Illite equilibria in solutions: I. Phase relationships in the system K_2O-Al_2O_3-SiO_2-H_2O between 25 and 250°C: *Geochim. et Cosmochim. Acta* **55,** 1353–1364.

Antweiler, R. C. and Drever, J. I. (1983) The weathering of a Late Tertiary volcanic ash: The importance of organic solutes: *Geochim. et Cosmochim. Acta* **47,** 623–629.

Bailey, S. W. (1980) Order-disorder in clay mineral structures: in *Crystal Structures of Clay Minerals and Their X-ray Identification,* G. W. Brindley and G. Brown, eds., Mineralogical Society, London.

Boles, J. R. (1992) Evidence for oil-derived organic acids in reservoirs: in *Proceedings of the 7th International Symposium on Water-Rock Interaction,* Y. K. Kharaka and A. S. Maest, eds., A. A. Balkema, Rotterdam, 311–314.

Brindley, G. W. (1980) Structure of layer silicates: in *Crystal Structures of Clay Minerals and Their X-ray Identification,* G. W. Brindley and G. Brown, eds., Mineralogical Society, London.

Burley, S. D. and Flisch, M. (1989) K-Ar geochronology and the timing of detrital I/S clay illitization and authigenic illite precipitation in the Piper and Tartan Fields, Outer Moray Firth, UK North Sea: *Clay Miner.* **24,** 285–316.

Chermak, J. A. and Rimstidt, J. D. (1990) The hydrothermal transformation rate of kaolinite to muscovite/illite: *Geochim. et Cosmochim. Acta* **54,** 2979–2990.

Cliff, G. and Lorimer, G. W. (1975) The quantitative analysis of thin specimens: *Journal of Microscopy* **103,** 203–207.

Cocker, J. D., Clauer, N., Tsui, T.-F., and Swarbrick, R. E. (1988) A diagenetic model for the Northwest Hutton field: in abstract volume, *Clay Diagenesis in Hydrocarbon Reservoirs and Shales,* Clay Minerals Group, Mineralogical Society, London, 5.

Crossey, L. J. (1991) Thermal degradation of aqueous oxalate species: *Geochim. et Cosmochim. Acta* **55,** 1515–1527.

Dove, P. M. and Crerar, D. A. (1990) Kinetics of quartz dissolution in electrolyte solutions using a hydrothermal mixed flow reactor: *Geochim. et Cosmochim. Acta* **54,** 955–969.

Giles, M. R. (1987) Mass transfer and problems of secondary porosity creation in deeply buried hydrocarbon reservoirs: *Marine and Petroleum Geology* **4,** 188–204.

Eberl, D. D. and Hower, J. (1976) Kinetics of illite formation: *GSA Bull.* **87,** 1326–1330.

Ehrenberg, S. N. (1991) Kaolinite-dickite transition in the Garn Formation, Haltenbanken: in *Proceedings of the 7th Euroclay Conference, Dresden 1991,* M. Storr, K.-H. Henning, and P. Adolphi, eds., European Clay Groups Association, Greifswald, 522.

Glasmann, J. R., Clark, R. A., Larter, S., Briedis, N. A., and Lundegard, P. D. (1989a) Diagenesis and hydrocarbon accumulation, Brent sandstone (Jurassic), Bergen High area, North Sea: *AAPG Bulletin* **73,** 1341–1360.

Glasmann, J. R., Lundegard, P. D., Clark, R. A., Penny, B. K., and Collins, I. D. (1989b) Geochemical evidence for the history of diagenesis and fluid migration: Brent Sandstone, Heather Field, North Sea: *Clay Miner.* **24,** 255–284.

Hamilton, D. L. and Henderson, C. M. B. (1968) The preparation of silicate compositions by a gelling method: *Mineralogical Magazine* **36,** 832–838.

Hamilton, P. J., Kelley, S., and Fallick, A. E. (1989) K-Ar dating of illite in hydrocarbon reservoirs: *Clay Miner.* **24,** 215–231.

Hogg, A. J. C., Fallick, A. E., and Pearson, M. J. (1991) Mapping diagenetic fluid flow within a reservoir-K/Ar dating in the Alwyn area, UK North Sea: *Program and Abstracts for Clay Minerals Society 28th Annual Meeting,* Houston, p. 74.

Howard, J. J. and Roy, D. M. (1983) Development of layer charge and kinetics of experimental smectite alteration: *Clays & Clay Minerals* **33,** 81–88.

Hower, J., Eslinger, E., Hower, M. E., and Perry, E. A. (1976) Mechanism of burial metamorphism of argillaceous sediments—1. Mineralogical and chemical evidence: *GSA Bull.* **87,** 725–737.

Huang, W. H. and Keller, W. D. (1970) Dissolution of rock-forming silicate minerals in organic acids: Simulated weathering of fresh mineral surfaces: *Amer. Mineral.* **55,** 2076–2094.

Huang, W. L., Bishop, A. M., and Brown, R. W. (1986) The effect of fluid/rock ratio on feldspar dissolution and illite formation under reservoir conditions: *Clay Miner.* **21,** 585–602.

Huang, W. L., Longo, J. M., and Pevear, D. R. (1991) An experimental derived kinetic model for smectite-to-illite conversion and its use as geothermometer: *Program and Abstracts for Clay Minerals Society 28th Annual Meeting,* Houston, p. 76.

Huertas, F. J., Huertas, F., and Linares, J. (1991) Activation energy of hydrothermal synthesis of kaolinite: in Proceedings of the 7th Euroclay Conference, *Dresden 1991,* M. Storr, K.-H. Henning, and P. Adolphi, eds., European Clay Groups Association, Greifswald, 533–537.

Inoue, A. (1983) Potassium fixation by clay minerals during hydrothermal treatment: *Clays & Clay Minerals* **31,** 81–91.

Lasaga, A. C. (1984) Chemical kinetics of water-rock interactions: *J. of Geophysical Research* **89,** 4009–4025.

Lee, M., Aronson, J. L., and Savin, S. M. (1989) Timing and conditions of Permian Rotliegende Sandstone diagenesis, southern North Sea: K/Ar and oxygen isotopic data: *AAPG Bull.* **73,** 195–215.

Macchi, L. (1987) A review of sandstone illite cements and aspects of their significance to hydrocarbon exploration and development: *Geol. J.* **22,** 333–345.

Macchi, L., Curtis, C. D., Levison, A., Woodward, K., and Hughes, C. R. (1990) Chemistry, morphology and distribution of illites from Morecambe Gas Field, Irish Sea, offshore United Kingdom: *AAPG Bull.* **74,** 296–308.

MacGowan, D. B. and Surdam, R. C. (1988) Difunctional carboxylic acid anions in oil-field waters: *Organic Geochem.* **12,** 245–259.

Nagy, K. L., Blum, A. E., and Lasaga, A. C. (1991) Dissolution and precipitation kinetics of kaolinite at 80°C and pH 3: The dependence on solution saturation state: *Amer. J. of Sci.* **291,** 649–686.

Rimstidt, J. D. and Barnes, H. L. (1980) The kinetics of silica-water reactions: *Geochim. et Cosmochim. Acta* **44,** 1683–1699.

Roberson, H. E. and Lahann, R. W. (1981) Smectite to illite conversion rates: Effects of solution chemistry: *Clays & Clay Minerals* **29,** 129–135.

Sass, B. M., Rosenberg, P. E., and Kittrick, J. A. (1987) The stability of illite/smectite during diagenesis: An experimental study: *Geochim. et Cosmochim. Acta* **51,** 2103–2115.

Scotchman, I. C., Johnes, L. H., and Miller, R. S. (1989) Clay diagenesis and oil migration in Brent Group sandstones of NW Hutton Field, UK North Sea: *Clay Miner.* **24,** 339–374.

Seyfried, W. E., Janecky, D. R., and Berndt, H. E. (1987) Rocking autoclaves for hydrothermal experiments II. The flexible reaction-cell system: in *Hydrothermal Experimental Techniques,* G. C. Ulmer and H. L. Barnes, eds., John Wiley, New York, 216–239.

Small, J. S. (1992) Clay precipitation from oxalate-bearing solutions: in *Proceedings of the 7th International Symposium on Water-Rock Interaction,* Y. K. Kharaka and A. S. Maest, eds., A.A. Balkema, Rotterdam, 345–348.

Small, J. S. (1993) An experimental study of the thermal and redox stability of dicarboxylic acid anions and their aluminium complexing behaviour: in *Proceedings of Geofluids 93, Torquay, England, 1993,* J. Parnell, A. Ruffell, and N. Moles, eds., Geological Society, London, 420–422.

Small, J. S., Hamilton, D. L., and Habesch, S. (1992a) Experimental simulation of clay precipitation in reservoir sandstones 1: Techniques and examples: *J. Sed. Petrol.* **62,** 508–519.

Small, J. S., Hamilton, D. L., and Habesch, S. (1992b) Experimental simulation of clay precipitation in reservoir sandstones 2: Mechanism of illite formation and controls on morphology: *J. Sed. Petrol.* **62,** 520–529.

Small, J. S. and Manning, D. A. C. (1993) Laboratory reproduction of morphological variation in petroleum reservoir clays: Monitoring of fluid composition during illite precipitation: in *Geochemistry of Clay Pore Fluid Interactions,* D. A. C. Manning, P. L. Hall, and C. R. Hughes, eds., Mineralogical Society/Chapman and Hall, London, 181–212.

Surdam, R. C., Boese, S. W., and Crossey, L. J. (1984) The chemistry of secondary porosity: in *Clastic Diagenesis,* D. A. McDonald and R. C. Surdam, eds., AAPG, Tulsa, 127–149.

Surdam, R. C., Crossey, L. J., Hagen, E. S., and Heasler, H. P. (1989) Organic-inorganic interactions and sandstone diagenesis: *AAPG Bull.* **73,** 1–23.

Warren, E. A. and Curtis, C. D. (1989) The chemical composition of authigenic illite within two sandstone reservoirs as analysed by ATEM: *Clay Miner.* **24,** 137–156.

Whitney, G. (1990) Role of water in the smectite-to-illite reaction: *Clays & Clay Minerals* **38,** 343–350.

Whitney, G. and Northrop, H. R. (1988) Experimental investigation of the smectite to illite reaction: Dual reaction mechanisms and oxygen-isotope systematics: *Amer. Mineral.* **73,** 77–90.

Wood, J. R. and Hewlett, T. A. (1982) Fluid convection and mass transfer in porous sandstones—A theoretical model: *Geochim. et Cosmochim. Acta* **46,** 1707–1713.

(Received 18 March 1993; accepted 19 March 1993; Ms. 2352)